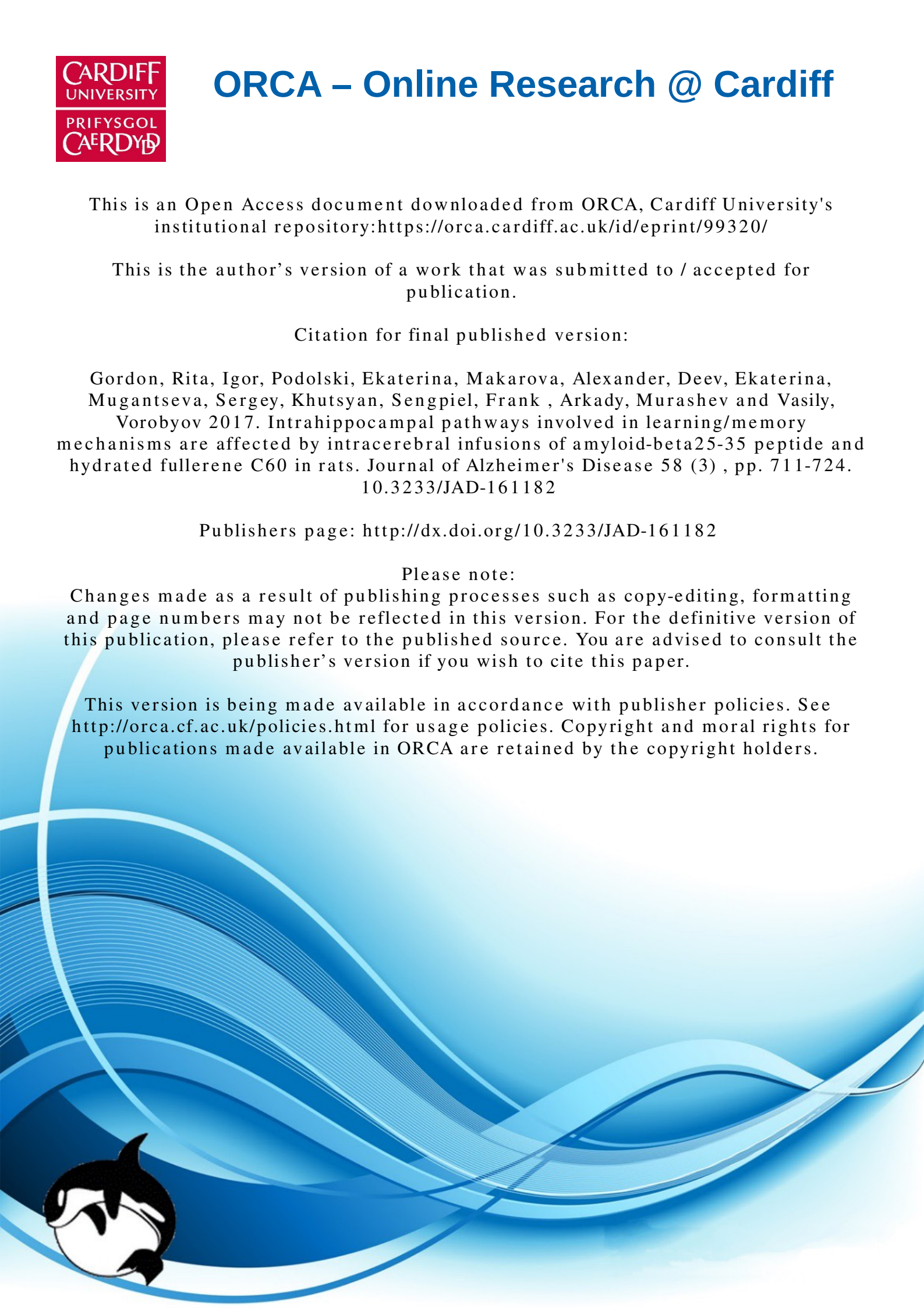

**Intrahippocampal pathways involved in learning/memory mechanisms are affected by intracerebral infusions of amyloid-beta$_{25-35}$ peptide and hydrated fullerene $C_{60}$ in rats**

Rita Gordon[a], Igor Podolski[b], Ekaterina Makarova[b], Alexander Deev[b], Ekaterina Mugantseva[b], Sergey Khutsyan[a,b], Frank Sengpiel[c], Arkady Murashev[d], Vasily Vorobyov[a]

[a]*Institute of Cell Biophysics, Russian Academy of Sciences, 142290 Pushchino, Moscow Region, Russia*
[b]*Institute of Theoretical and Experimental Biophysics, Russian Academy of Sciences, 142290 Pushchino, Moscow Region, Russia*
[c]*School of Biosciences and Neuroscience & Mental Health Research Institute, Cardiff University, Museum Avenue, Cardiff CF10 3AX, UK*
[d]*Branch of Shemyakin & Ovchinnikov Institute of Bioorganic Chemistry, Russian Academy of Sciences, 142290 Pushchino, Moscow Region, Russia*

**Running head:** *Intrahippocampal pathways vs. Learning/Memory*

**Corresponding author:**

Dr. V. Vorobyov, PhD
Institute of Cell Biophysics
Pushchino, 142290, Russia
Tel: 007-4967-739-223
Fax: 007-4967-330-509
E-mail: vorobyovv2@gmail.com

Dr. R. Gordon, PhD
Institute of Cell Biophysics
Pushchino, 142290, Russia
Tel: 007-4967-739-305
Fax: 007-4967-330-509
E-mail: ritagordon@yandex.ru

**Abstract**

Primary memory impairments associated with increased level of amyloid-beta (Aβ) in the brain have been shown to be linked, partially, with early pathological changes in the entorhinal cortex (EC) which spread on the whole limbic system. While the hippocampus is known to play a key role in learning and memory mechanisms, it is as yet unclear how its structures are involved in the EC pathology. In this study, changes in memory and neuronal morphology in male Wistar rats intrahippocampally injected with $A\beta_{25-35}$ were correlated on days 14 and 45 after the injection to reveal specific cognitive - structural associations. The main focus was on the dentate gyrus (DG) and hippocampal areas of CA1 and CA3 because of their involvement in afferent flows from EC to the hippocampus through tri-synaptic (EC → DG → CA3 → CA1) and/or mono-synaptic (EC → CA1) pathways. Evident memory impairments were observed at both time points after $A\beta_{25-35}$ injection. However, on day 14, populations of morphological intact neurons were decreased in CA3 and, drastically, in CA1, and the DG supramedial bundle was significantly damaged. On day 45, this bundle largely and CA1 neurons partially recovered, whereas CA3 neurons remained damaged. We suggest that $A\beta_{25-35}$ primarily affects the tri-synaptic pathway, destroying the granular cells in the DG supramedial area and neurons in CA3 and, through the Schaffer collaterals, in CA1. Intrahippocampal pretreatment with hydrated fullerene $C_{60}$ allows the neurons and their connections to survive the amyloidosis, thus supporting the memory mechanisms.

**Key words**: hippocampus; CA1; CA3; dentate gyrus; neurodegeneration; Alzheimer's disease

## 1. Introduction

Spatial orientation and memory in rodents are associated with the structural and functional organization of the hippocampus [1]. The "spatial map" in the hippocampus has been proposed to allow the estimation of movement direction and the calculation of the distance between objects in the environment [2]. At the neuronal level, the "maps" are organized by specific distribution of neuronal nets analyzing and integrating spatial landmarks. The specificity both of various hippocampal areas - CA1, CA3, and dentate gyrus (DG) - which differ in their sensitivity to disturbing factors, and of their connections, are of particular interest. Amyloid-beta (Aβ) peptides, an Alzheimer's disease (AD) hallmark, are one of such factors. The soluble Aβ oligomers in AD patients have been shown to consist of $A\beta_{1–40}$ or $A\beta_{1–42}$ [3] and $A\beta_{25–35}$, which is generated by enzymatic cleavage of $A\beta_{1–40}$ [4]. Interest in $A\beta_{25–35}$ is associated with its capability to disturb neurons, and their functions, synaptic plasticity, and memory [5]. Substantial impairments in spatial orientation and memory were observed in a rat model of AD with intracerebral injection of $A\beta_{25-35}$ [6], [7]. In studies evaluating Aβ -induced memory disturbances in rodents, protective effects of fullerene $C_{60}$-type nano-compounds with anti-oxidative and anti-aggregative activities were revealed [8]. Intrahippocampal injection of a hydrated fullerene $C_{60}$ ($C_{60}$HyFn) improved the spatial memory in rats with disturbed peptide synthesis [9], whereas carboxy-fullerene, did the same in old mice [10]. $C_{60}$HyFn has been shown to protect spatial memory from $A\beta_{25-35}$-induced toxicity in rats [11] and to activate long-term potentiation (LTP) [12].

An analysis of primary *vs.* secondary $A\beta_{25-35}$ effects on learning/memory and neuronal morphology in different brain areas might be a universal approach for the evaluation of changes in the neuronal networks involved in the amyloidogenic pathology [13]. Two main afferent pathways (tri-synaptic: EC → DG → CA3 → CA1, and monosynaptic: EC → CA1) connect the entorhinal cortex, closely associated with the early/primary memory disturbances in AD [3], [14], with the hippocampus. Which of them might be predominantly involved in the $A\beta_{25-35}$ neurotoxic effects on memory mechanisms?

Recently, we have shown that after intrahippocampal injection of $A\beta_{25-35}$, its cytoplasm deposits in pyramidal neurons were visible on day 14, in spite of immediate and long-lasting decrease of protein synthesis [15]. Disturbances in behavioral, physiological, biochemical and morphological characteristics in rats were observed even six weeks after injection of $A\beta_{25-35}$ into cerebral ventricles [16] while its toxicity has been shown to be eliminated by $C_{60}$HyFn pretreatment [17]. Peculiarities of cortical-hippocampal nets involvement in the long-term effects of enhanced Aβ level in the brain and in their treatment with $C_{60}$HyFn are the main targets in this study.

## 2. Materials and Methods

*2.1 Animals*

Ninety eight male Wistar rats (290-330 g), bred at the AAALAC accredited Pushchino Animal Breeding Facility (Russia) from colonies obtained as a courtesy from Harlan UK Ltd., were used in this study. The animals were kept in a standard regime, with food and water ad libitum and a 12-h/12-h day/night cycle. The procedures were carried out in accordance with the principles enunciated in the Guide for Care and Use of Laboratory Animals, NIH publication No 85-23, and approved by IACUC of the Institute of Cell Biophysics.

*2.2. Intrahippocampal infusions*

Anesthesia was induced with subcutaneous (s.c.) injection of tiletamine/zolazepam (Zoletil®, Virbac, France) in combination with xylazine (Rometar®, Bioveta, Czech Republic) at doses of 25 mg/kg and 1 mg/kg, respectively. Saline, $C_{60}$HyFn (at 0.5 nmol/μl), $A\beta_{35-25}$, and $A\beta_{25-35}$ protein (Sigma, USA, at 2 nmol/μl), in volumes of 1.5–2.0 μl, were slowly infused (for ~2 min) symmetrically into hippocampal CA1 areas (AP −3.8, L 2.5, H 3.5) [18]. These areas have been shown in our previous study to be preferential target for $A\beta_{25-35}$ injected *into the brain lateral ventricles* [15]. Moreover, CA1 areas seem to be specifically sensitive to $A\beta_{25-35}$ as *greatly delayed* pathological changes in CA1 *vs*. CA3 were observed after intoxication of CA1 with kainate [19]. Fullerene $C_{60}$HyFn was obtained courtesy of Dr. G. Andrievsky who developed this highly stable water-soluble form of the fullerene $C_{60}$ (MER Corp, USA) [20]. A temporarily inserted guide cannula (blunt stainless steel needle, 0.8 mm inner diameter) with flexible silastic tubing attached to a 5-μl Hamilton syringe was used for the infusion. The needle was kept in place for 3 min before withdrawal. Before injection of $A\beta_{25-35}$, aliquots were defrosted and incubated at 37°C for two days to aggregate the protein into fibrils [21] that were assessed by electron microscopy (x50000). The cannula tip positions were verified *post mortem* in paraffin hippocampal slices of 40 μm in thicknesses, which were stained with cresyl violet (Sigma-Aldrich, St. Louis, USA). Five groups of rats with two intrahippocampal injections (2 h apart) were studied. They were arbitrarily allocated to Saline + Saline and Saline + $A\beta_{35-25}$ (as controls, n = 22 and 9), Saline + $A\beta_{25-35}$, $C_{60}$HyFn + Saline, and $C_{60}$HyFn + $A\beta_{25-35}$ (n = 27, 12, and 28, respectively). Recently, we have shown that two weeks after intrahippocampal injections of the fullerene or saline, no morphologically visible injuries of the brain tissue were observed [17]. Given these, in our present study, a simplified (rough) morphological examination was only performed to exclude an accidental damage of the hippocampus during manipulations with the cannula.

*2.3 Spatial discrimination testing*

Two weeks after intrahippocampal injections, the learning/memory abilities of the rats were tested with the Morris water maze paradigm [22] in a circular water pool (diameter, 150 cm; height, 80 cm), filled to a depth of 50 cm with water (25°C) made opaque with powdered

milk. On Day 13, the locomotor ability of each rat was evaluated by the latency of their reaching a *visible* platform (5 cm above the water surface, 9 cm in diameter) located in one of quadrants. This task provided a measure of basic swimming ability to escape from water and required no searching, hence no learning, ensuring that all animals used in the study were initially equivalent across groups prior to further trials in learning and memory tasks [23].

On Days 14 and 21, the rats from different groups (Saline + Saline, Saline + $A\beta_{35-25}$, Saline + $A\beta_{25-35}$, and $C_{60}$HyFn + $A\beta_{25-35}$; n = 7, 9, 12, and 13, respectively) were trained over 4 trials to reach the platform that was submerged 0.5 cm below the surface and invariably located in one of the pool's quadrants (Session I). The animals were allowed a maximum of three minutes to find the platform followed by a 20-s rest period, once on the platform, before being dried and relocated into the home cage. An unsuccessful rat was gently redirected to the platform after exceeding the exploratory time limit. On Day 21, one hour after the training/learning session was complete, a 60-s probe trial, with the platform temporarily removed from the pool, was given to assess the *short-term memory*, retaining spatial information about the target quadrant. To assess the *long-term memory* the second probe trial was performed two days (48 hrs) later. Escape latency in the training sessions and total time spent in the target quadrant (during the probe trial) were computed using an in-house developed video tracking system with a digital camera (Logitech QuickCam 3000, 800x600 pixels, 15 fps) located 2.5 m above the pool. On Days 28, 35, and 42, the rats experienced a *reversal learning* (Sessions II, III, and IV, respectively) of 4 trials with the hidden platform in another quadrant, individually for each rat across the days. Both probe trials (1.0 h and 48 hrs after the training trials) and 5-day resting intervals were included in the protocol of these sessions as well. The resting for several days allows analyzing the animal's capability to develop some kind of "*episodic*" memory associated with retaining spatial information in the interval *between* the consecutive sessions. The mechanism activated by this assay seems to be involved in rapid "*one-trial learning*" closely associated with synaptic plasticity [24].

*2.4 Morphological and histochemical evaluations of neuronal viability*

In additional groups of Saline + Saline, Saline + $A\beta_{25-35}$, $C_{60}$HyFn + Saline, and $C_{60}$HyFn+$A\beta_{25-35}$ (n = 12, in each group), we evaluated the distribution of morphologically intact pyramidal neurons in hippocampal slices on Day 14 and Day 45. $A\beta_{25-35}$ was chosen since this peptide, usually used in a synthetic form, replicates $A\beta_{1-42}$ toxicity [25], [26], and, on the other hand, it is not involved directly in recovery mechanisms associated with $A\beta_{1-42}$ [27]. After decapitation under diethyl ether, one hemisphere was fixed in Carnow's mixture (ethanol, chloroform, and acetic acid, at ratios of 6:3:1, respectively), whereas another one was put in 4% paraformaldehyde with PBS and then embedded in paraffin. The brain blocks were sectioned on Leica's microtome (Germany), and prepared 7-μm slices were used for different (light, immunohistochemical and fluorescent) assessments.

*2.4.1 Light microscopy*

Characterization of the pyramidal neurons in CA1 and CA3 was performed on brain slices *Nissl* stained with cresyl violet (Sigma-Aldrich, St. Louis, USA) to mark intracellular RNA in both the endoplasmic reticulum, the nucleus and other intracellular structures containing nucleic acids that in turn allows the evaluation of changes in morphological organization of neurons [28]. From each animal, 25–30 brain slices were scanned and transferred through a digital camera to Axio Imager M1 optical microscope (Zeiss, Germany). Further analyses of 200x50 μm (0.01 $mm^2$) frames was performed with use of Image J1.44 software (USA) that allowed the separation of damaged from intact neurons. In this study, we accounted only *morphologically intact neurons* characterized by uniformly colored cytoplasm and nucleoplasm, sharpened plasmatic and nuclear membranes, and clearly defined nucleus and nucleolus.

*2.4.2 Immunohistochemical analysis*

In our previous study, we have demonstrated close association between distributions of surviving cells and diffuse $A\beta_{1-42}$ deposits in neurons [29]. In present study we evaluated the deposits on 12 rats (three animals from each group) aiming to use obtained evidence in peculiar supplemental analysis of the light microscopy results. The immunohistochemical analysis was performed accordingly to a standard technique [30]. To enhance sensitivity to Aβ the brain slices were treated with 70% formic acid for 4 min, whereas to block the endogenous peroxidase activity, they were incubated in 0.5% $H_2O_2$/ethanol mixture, and 5% normal goat serum was used to block unspecific binding. The sections were further incubated with primary antibodies: rabbit polyclonal anti-$A\beta_{1-40}$ (1:400, Sigma) at a temperature of +4◦C for 15 h. The antibodies were recognized by anti-rabbit IgG (1:800, Sigma) and identified by StreptABComplex/HRP (1:800, Sigma). The reaction was visualized with use of 3,3'-diaminobenzidine. For control sections, the primary antibodies were replaced with PBS. (For more details, see [17]).

*2.4.3 Fluorescent microscopy*

Fluoro-Jade B (Millipore) staining [31], in its modified version, was performed to characterize irreversibility of neuronal degeneration with aim to use obtained evidence in peculiar supplemental analysis of the light microscopy results. Dehydrated slices were immediately transferred to 0.06% solution of potassium permanganate, where they were kept for 30 min at RT and then stained by freshly prepared 0.0001% solution of Fluoro-Jade B in 0.1% acetic acid for 25 min. After final preparation (washing in distilled water, drying, clearing in xylene, and covering by glass slides), the slices were examined with use of DM 6000 fluorescent microscope (Leica).

*2.5. Statistics*

The results of the Morris test were analyzed using the two-way repeated measures ANOVA and non-parametric Mann-Whitney U-test, with preliminarily performed Shapiro-Wilks test and Greenhouse-Geisser correction, followed by Bonferroni post hoc analysis for multiple comparisons. The immunohistochemical and morphometric data were analyzed by non-parametric Mann-Whitney U-test with Bonferroni correction. The group data were expressed as the means ± SEM; differences were considered significant at $p < 0.05$. The statistical analyses were performed using STATISTICA (data analysis software system), version 10 (StatSoft, Inc., Tulsa, OK, USA).

## 3. Results

*3.1 Learning and memory*

In the first trial of initial learning session I on Day 14, latencies of finding the submerged platform were variable between different groups; nevertheless, the variability did not reach significant values (Fig. 1, A, B). In the second trial, the rats intrahippocampally injected with saline showed significantly shorter latency compared with animals from other groups. Furthermore, despite obvious *trial-by-trial* trends in these groups, only rats treated with $C_{60}$HyFn reached the platform sufficiently quickly in the 4$^{th}$ trial. Therefore, the first session (Fig. 1, A, B, 1 - 4 trials) was extended by additional four trials on Day 21 (Fig. 1, A, B, 5 - 8 trials) that finally minimized the latencies in all groups, making them comparable in the end of the session. Despite all rats learned to perform the task, their progression profiles were evidently different in animals from Saline + A$\beta_{25-35}$ group *vs.* those from groups of Saline + Saline, Saline + A$\beta_{35-25}$, and $C_{60}$HyFn + A$\beta_{25-35}$ (Fig. 1, A, B), that was confirmed by 2-way ANOVA ($F_{1,136} = 81.3$, $p < 0.001$, $F_{1,144} = 18.9$, $p < 0.01$, and $F_{1,184} = 69.3$, $p < 0.001$, respectively). The latter highlights the beneficial effect of the fullerene on A$\beta_{25-35}$-induced disturbances in learning. Nevertheless, the traces of these disturbances (slightly increased latencies) were observed in other sessions (Fig. 1, B). The inhibitory effect of A$\beta_{25-35}$ on learning was robustly expressed in rats from Saline + A$\beta_{25-35}$ group in all training trials *vs.* those in animals from Saline + Saline, Saline + A$\beta_{35-25}$, or $C_{60}$HyFn + A$\beta_{25-35}$ groups (2-way ANOVA: $F_{1,68} = 84.2$, $F_{1,76} = 70.1$, or $F_{1,92} = 78.3$, respectively, $p < 0.001$, for all groups). The elimination of the detrimental effect of A$\beta_{25-35}$ on memory by $C_{60}$HyFn was evidently shown on the plots of escape latencies averaged for each session (Fig. 1, C, D). The rats from $C_{60}$HyFn + A$\beta_{25-35}$ group reached the platform significantly faster than those from Saline + A$\beta_{25-35}$ group (2-way ANOVA: $F_{1,92} = 61.1$, $p < 0.001$) while the latencies in $C_{60}$HyFn + A$\beta_{25-35}$ group *vs.* other groups were comparable (2-way ANOVA: $F_{1,72} = 1.3$ or $F_{1,80} = 0.8$, for Saline + Saline or Saline + A$\beta_{35-}$, respectively, $p < 0.05$, for all groups). In the probe/testing sessions

performed 1 h and 48 hrs after the training ones (Fig. 1, E, F), significant differences between Saline + $A\beta_{25-35}$ and Saline + Saline or Saline + $A\beta_{35-25}$ (2-way ANOVA: $F_{1,136} = 58.3$ or $F_{1,152} = 47.5$, respectively, $p < 0.001$, for all groups) were revealed. This detrimental effect of $A\beta_{25-35}$ was not observed in rats pretreated with $C_{60}$HyFn + $A\beta_{25-35}$ *vs.* Saline + Saline or Saline + $A\beta_{35-25}$ (Fig. 1, F; 2-way ANOVA: $F_{1,144} = 0.8$ or $F_{1,160} = 1.1$ , respectively, $p > 0.05$, for all groups). Given inefficacy of $A\beta_{35-25}$ treatment in behavioral tests, further morphological and histochemical study was performed on rats from groups of Saline + Saline, Saline + $A\beta_{25-35}$, $C_{60}$HyFn + Saline, and $C_{60}$HyFn + $A\beta_{25-35}$.

*3.2 Morphology of hippocampal neurons*

The undamaged state of hippocampal neurons is crucial for learning/memory mechanisms functioning [32], [33]. In our study, the morphology of neurons from different areas of the hippocampus (Fig. 2) was analyzed after intrahippocampal injection of $A\beta_{25-35}$ in rats that has been shown above to produce robust disturbances in their learning/memory abilities (Fig. 1).

On Day 14 after the injection, a vast of swelled and vacuolated neurons with indistinct and rupture cell and nuclear membranes, and subsequent loss of intracellular components, typical features of necrosis [34], were observed in CA1 (Fig. 3, A) and in CA3 (predominantly in CA3a) (Fig. 4), with expectable decreased population of morphologically intact neurons in these hippocampal areas (Fig. 5). DG suprapyramidal bundle was evidently damaged (Fig. 6, A). Pretreatment with fullerene $C_{60}$HyFn, 2 h prior to $A\beta_{25-35}$, largely prevented neurodegenerative changes in CA1 (Fig. 3, B) and in CA3 (not shown) that was statistically supported by evident increase of the intact cells populations (Fig. 5). DG suprapyramidal bundle was partially preserved as well (Fig. 6, C).

On Day 14 after intrahippocampal infusion of $A\beta_{25-35}$, immunohistochemical analysis revealed diffuse $A\beta_{1-42}$ deposits in the cytoplasm of CA1 pyramidal neurons (Fig. 7, A). Nevertheless, *Fluoro-Jade B* staining, identifying irreversible cell damage, demonstrated fluorescence in both CA1 (Fig. 7, B), DG (Fig. 8, A) and CA3 (Fig. 8, B). In DG, *Fluoro-Jade B* staining was captured by both glia and degenerated neurons, especially, in the supra- *vs.* infrapyramidal bundles (Fig. 8, A). It should be mentioned, however, that in both CA1 (Fig. 7, B) and CA3 (Fig. 8, B) the fluorescence was observed only around, rather than inside, the bodies of pyramidal neurons, supposedly, in glia. In contrast, no fluorescence was detected in rats from Saline + Saline and $C_{60}$HyFn + $A\beta_{25-35}$ groups with significant decrease of $A\beta_{1-42}$ deposits in neurons [29]. Thus, accumulation of endogenic Aβ in cytoplasm of CA1 neurons was accompanied by a decreased population of the intact neurons (see Fig. 5) but, surprisingly, by a lack of *Fluoro-Jade B* labeled (i.e., damaged) neurons (Fig. 7, B).

On Day 45, population of morphologically intact CA1 neurons in rats from Saline + $A\beta_{25-35}$ group was bigger than that on Day 14 (Fig. 9 *vs.* Fig. 5). This supports the suggestion that neurodegeneration in CA1 seems to be partially reversible. In contrast, population of

morphologically intact CA3 neurons in rats from this group was smaller than that observed on Day 14 (Fig. 9 *vs.* Fig. 5; Fig. 10, A). On Day 45 after $C_{60}$HyFn + $A\beta_{25-35}$ injection, populations of morphologically intact cells in CA1 and CA3 were kept at relatively high levels, comparable with those observed on Day 14 (Fig. 9 *vs.* Fig. 5; Fig. 10, B). Thus, in spite of different trends in evolution of morphologically normal cells populations in CA1 and CA3 in Saline + $A\beta_{25-35}$ group, the pretreatment with fullerene $C_{60}$HyFn rescued these populations completely in CA1 and partially in CA3 (Fig. 9 *vs.* Fig. 5). On Day 45 *vs.* Day 14, DG suprapyramidal bundle was restored in rats from both Saline + $A\beta_{25-35}$ group, completely (Fig. 6, B *vs.* Fig 6, A), and $C_{60}$HyFn + $A\beta_{25-35}$ group, partially (Fig. 6, D *vs.* Fig. 6, C).

**4. Discussion**

In our study, on days 14 and 45 after a single intrahippocampal injection of $A\beta_{25-35}$ in rats, different types of memory (operative, episodic, and long-term) were impaired. Unaffected functioning of short-term memory only was observed exclusively on day 14. Since each of these types of memory is associated with complex interactions between multiple neuronal nets, it is difficult to isolate a role of individual brain structure which might be crucial for the memory impairment. Instead of individual structures supporting specific brain functions, it is more likely that neurons activated by a particular task are widely distributed across the brain.

In the present study, we correlate disturbances in memory of different types and morphological changes in hippocampal CA1, CA3, and dentate gyrus, which have been shown to be involved in organization of tri- and mono-synaptic pathways. The former, entorhinal cortex (EC) $\rightarrow$ dentate gyrus (DG) $\rightarrow$ CA3 $\rightarrow$ CA1, seems to be associated with the storing of new events, whereas the latter, EC $\rightarrow$ CA1, is associated with previously fixed events [14], [35]. They both converge on single pyramidal cells of the CA1, but affecting them differently. Interestingly, in AD and in its "amyloid-beta" models, early degenerative changes were revealed in CA1 pyramidal neurons [14], [15], [17], [29], [36]. A primary target of Aβ is the EC which, being the main cortical input for the hippocampus, plays a considerable part in memory formation [3], [8], [14], [37]. In AD-associated neurodegeneration, EC is affected first, before evident disturbances in cognition and behavior [38]. The second layer of EC plays an important role in animal navigation and provides tri-synaptic afferent connection to DG and hippocampal CA3 and CA1 areas. In addition, medial EC is connected predominantly with the infra-pyramidal branch of DG, whereas lateral EC does the same with its supra-pyramidal branch [39], [40]. The third layer of EC is connected directly with CA1 through the mono-synaptic pathway [41]. The tri-synaptic pathway is well known to be extremely sensitive to Aβ-induced disturbances at early stage of AD that is expressed both in dramatic loss of neurons in the second (*vs.* the third) layer of EC and in pathological modifications of the granular cells in DG, CA3, and CA1 [14].

We have shown that on day 14 after the Aβ injection the hippocampal neurons were damaged both in CA1 and, to a lesser extent, in CA3 (Fig. 5 and Fig. 9, respectively). *Fluoro-Jade B* staining reveals both the glial cells and degenerating neurons in ischemia [42] and after single injection of a neurotoxin, kainate [19], [31], [43]. Thus, a lack of *Fluoro-Jade B* markers on CA1 neurons in our study might be associated either with a regenerative capability of the neurons or with co-localization of the markers and Aβ that produced a "masking" effect [44]. Indeed, a population of morphologically uninjured neurons was increased on day 45 after $A\beta_{25-35}$ injection (Fig. 9); this may be associated with the reversibility of neurodegenerative processes. On the other hand, given *Fluoro-Jade B* specificity to stain both reactive astroglia and microglia in neurodegeneration [44] it is reasonable to expect that $A\beta_{25-35}$ injection was able to initiate inflammation, typical for AD [45], [46].

On day 14, the suprapyramidal bundle to DG, closely associated with separation of new and old information [40], completely disappeared (Fig. 6, A). In this respect, our data are in line with evidence about high sensitivity of this bundle (a projection of the lateral EC) to AD, especially at its early stages [47], [48]. In contrast, the infrapyramidal DG (a projection of the medial EC) was practically unaffected (Fig. 6, A), and this was accompanied by normal short-term memory processing. On the other hand, the medial EC is well known to be unnecessary for many types of hippocampus-dependent memory; however, it is important for spatial memory [49]. It should be mentioned that the suprapyramidal bundle terminates in the distal area of CA3, in CA3a, whereas the infrapyramidal bundle terminates in the proximal area of CA3, in CA3c [39], [40]. Therefore, it can be expected that elimination of the suprapyramidal bundle results in deafferentation of CA3a, and, as a consequence, in more powerfully expressed degeneration of its neurons *vs.* those in CA3c (Fig. 4).

Thus, the neurodegeneration-causing factors (Aβ, in particular) initiate a primary (on day 14, in our study) damage of the lateral part of the second layer of EC, the subpyramidal bundle of DG, degeneration predominantly CA3 neurons, and, finally, powerfully expressed degeneration of CA1 neurons. This is accompanied by disturbances in operative, episodic, and long-term types of memory without any influence on short-term memory (Fig. 1, E, F). In rats, both operative, short- and long-term memories need normal functioning of several limbic system components: the hippocampus, DG, and EC [50]. In contrast to long-term memory, the mechanism of consolidation, associated with the hippocampus [51], is not involved in short-term memory [52], which explains its insensitivity to Aβ, observed in our study. Functional disturbances in neuronal circuits are associated with different pathological causes (loss of neurons, synapses, and connections between them); they may be expressed in LTP inhibition. These effects are typical for chronic treatment with pathogenic factors and/or neurodegenerative diseases [53]. In the prolonged time interval (day 45) after the $A\beta_{25-35}$ injection, there was both (partial) recovery of CA1 neurons and of the suprapyramidal bundle

of DG and, paradoxically, a decrease of morphologically normal neuron population in CA3 (Fig. 9 and Fig. 10, A). In parallel, significant disturbances in all analyzed types of memory were observed (Fig. 1, E, F). These evoke the question about relative role of DG and CA3 neurons in memory recovery in prolonged interval after Aβ injection. Freshly generated granular cells have been shown to play an extremely important role in the neuronal circuits associated with spatial memory [54]. Furthermore, inhibition of granular cell neurogenesis has been shown to affect negatively learning and memory in rats [33]. Interestingly, granular cells maturation in the DG of dorsal hippocampus takes a relatively long time (30 days) [55]. Thus, it is reasonable to hypothesize that the disturbances of neurogenesis revealed in our study are caused by Aβ-induced elimination of the network connections between EC and new granular cells and by failure of their recovery [14], [56] that is especially critical for functioning of CA3 neurons and, in turn, of memory mechanisms. In both transgenic mice and AD patients, synaptic disturbances have been shown to be the main source of cognitive dysfunctions, such as Aβ-induced inhibition of LTP and induction of long-lasting depression, both closely associated with memory loss [14], [41]. Bearing in mind that inhibition of synaptic plasticity is negatively correlated with the ability to process new information [57], and that the tri-synaptic pathway is supposedly involved in its storage, a synaptic pathology might be a reasonable cause of memory weakening [14], [35]. The prolonged Aβ effect seems to be associated with involvement of the tri-synaptic pathway, firstly targeting CA3 neurons and then, through the Schaffer collaterals, CA1 neurons.

The neuroprotective role of fullerene $C_{60}$HyFn, revealed in our study, was expressed in prevention of both memory impairment and neuronal damage produced by intrahippocampal $A\beta_{25-35}$ injection. This protective effect was observed both at early stage (day 14) of $A\beta_{25-35}$-induced neurotoxicity and much later, on day 45. Fullerenes are well known to be characterized by their powerfully expressed antioxidant and antiamyloid activities [10], [11], [58], [59], [60]. Recently, we have shown that intrahippocampal injection of $C_{60}$HyFn was able to protect both the mechanisms of peptide synthesis and amyloid accumulation, and CA1 neurons in rats from neurotoxic effects of the intracerebral injection of $A\beta_{25-35}$ [17]. Furthermore, fullerenes used at low dose have been shown to increase the survival rate of hippocampal neurons [61], and $C_{60}$HyFn, injected at low dose into the hippocampus, significantly improved both LTP and spatial memory in rats [12], usually accompanied by an increased ratio of postsynaptic AMPA and NMDA receptors. AMPA receptors have been shown to be involved in potentiation of activation of both alpha-secretase and non-amyloidal path of an amyloid precursor (APP) cleavage, i.e., without formation and accumulation of extremely toxic $A\beta_{1-42}$ [62]. In our previous study, we have revealed $C_{60}$HyFn-produced inhibition of intracellular $A\beta_{1-42}$ deposit formation associated with exogenous fibrillar $A\beta_{25-35}$ [29] and, supposedly, with its endogenous fullerene-disaggregated form [11]. $C_{60}$HyFn ability to block both intracellular $A\beta_{1-42}$ generation and the extracellular glutamate receptors activity

[63] reducing $Ca^{2+}$ inflow, one of the main sources of $A\beta_{25-35}$ neurotoxicity [64]). These mechanisms are expected to "intercept" the development of the $A\beta_{25-35}$-associated effects and, in that way, protecting the network connections between different hippocampal areas, survival rate of their neurons, and, finally, memory functioning. The paradoxical discrepancy between inhibitory effect of $C_{60}$HyFn on neurogenesis of granular cells in DG (Fig. 6, D) and a lack of changes in memory (Fig. 1, E, F) needs to be analyzed in further studies. This might be associated with a cytotoxic effect of $C_{60}$HyFn [65] on DG, the brain region characterized by powerfully expressed neurogenesis in adulthood [55], and/or with DG suprapyramidal bundle involvement in particular types of hippocampus-dependent learning/memory mechanisms [57].

## 5. Conclusions

Learning/memory mechanisms are well known to be dependent on the functional relationships between the cortex and multiple areas of the hippocampus. We have shown that memory disturbances evoked by experimental degeneration in the brain are predominantly associated with one of hippocampal areas, CA3. Furthermore, we have demonstrated that some of nano-compounds (in particular, hydrated fullerenes) are able to fight against the neurodegeneration, thus supporting the memory mechanisms. Finally, the morpho-functional approach used in our study and obtained data allow the understanding of pathophysiological mechanisms of brain structural and functional connectivity disruption in AD progression revealed in MRI studies [66], [67].

**Acknowledgments:** This work was supported by a grant of Russian Fund of Basic Research #15-04-05463.

**Conflict of Interest:** The authors declare that they have no conflict of interest.

**References**


[1] Wood ER, Dudchenko PA (2003) Aging, spatial behavior and the cognitive map. *Nat.Neurosci* **6**, 546–548.

[2] O'Keefe J, Burgess N (1996) Geometric determinants of the place fields of hippocampal neurons. *Nature* **381**, 425–428.

[3] Haass C, Selkoe DJ (2007) Soluble protein oligomers in neurodegeneration: lessons from the Alzheimer's amyloid beta-peptide. *Nat Rev Mol Cell Biol* **8**, 101-112.

[4] Kaneko I, Morimoto K, Kubo T (2001) Drastic neuronal loss in vivo by bamyloid racemized at Ser(26) residue: Conversion of non-toxic [D-Ser(26)]Ab 1–40 to toxic and proteinase-resistant fragments. *Neuroscience* **104**, 1003–1011.

[5] Varadarajan S, Kanski J, Aksenova M, Lauderback C, Butterfield DA (2001) Different mechanisms of oxidative stress and neurotoxicity for Alzheimer's Ab(1–42) and Ab(25–35). *J Am Chem Soc* **123**, 5625–5631.

[6] Chen G, Chen KS, Knox J et al (2000) A learning deficit related to age and beta-amyloid plaques in a mouse model of Alzheimer's disease. *Nature* **408**, 975-979.

[7] Morris RG (2001) Episodic-like memory in animals: psychological criteria, neurl mechanisms and the value of episodic-like tasks to investigate animal models of neurodegenerative disease. *Philos Trans R Soc Lond B Biol Sci* **356**, 1453-1465.

[8] Citron M (2010) Alzheimer's disease: strategies for disease modification. *Nat Rev Drug Discov* **9**, 387-398.

[9] Podolski IYa, Kondratjeva EV, Gurin SS, Dumpis MA, Piotrovsky LB (2004) Fullerene C60 complexed with poly(N-vinyl-pyrrolidone) (C60/PVP) prevents the disturbance of long-term memory consolidation induced by cycloheximide. *Fullerenes, nanotubes, carbon nanostructures* **12**, 443-446.

[10] Quick K L, Ali SS, Arch R, Xiong C, Wozniak D, Dugan LL (2008) A carboxyfullerene, S. O. D. mimetic improves cognition and extends the lifespan of mice. *Neurobiol Aging* **29**, 117–128.

[11] Podolski IYa, Podlubnaya ZA, Kosenko EA et al (2007) Effects of hydrated forms of C60 fullerene on amyloid 1-peptide fibrillization in vitro and performance of the cognitive task. *J Nanosci Nanotechnol* **7**, 1479-1485.

[12] Chen L, Miao Ya, Chen Lin et al (2014) The role of low levels of fullerene C60 nanocrystals on enhanced learning and memory of rats through persistent CaMKII activation. *Biomaterials* **35**, 9269-9279.

[13] Yamamoto K, Tanei Z, Hashimoto T, Wakabayashi, T, Okuno H, Naka Y, Yizhar O, Fenno LE, Fukayama M, Bito H, Cirrito JR, Holtzman DM, Deisseroth K, Iwatsubo T (2015) Chronic optogenetic activation augments aβ pathology in a mouse model of Alzheimer disease. *Cell Rep* **11**, 859-865.

[14] Llorens-Martin M, Blazquez-Llorca L, Benavides-Piccione R, Rabano A, Hernandez F, Avila J, DeFelipe J (2014) Selective alterations of neurons and circuits related to early memory loss in Alzheimer's disease. *PERSPECTIVE ARTICLE Frontiers in Neuroanatomy* **8**, 1-12.
[15] Gordon RYa, Makarova EG, Podolski IYa, Rogachevski VV, Kordonets OL (2012) Impairment of protein synthesis is early effect of amyloid-β in neurons. *Neurochem J* **6**, 121-131.
[16] Zussy C, Brureau A, Keller E et al (2013) Alzheimer's disease related markers, cellular toxicity and behavioral deficits induced six weeks after oligomeric amyloid-β peptide injection in rats. *PLoS One* **8**, e53117. doi: 10.1371/journal.pone.0053117.
[17] Makarova EG, Gordon RY, Podolski IY (2012) Fullerene C60 prevents neurotoxicity induced by intrahippocampal microinjection of amyloid-beta peptide. *J Nanosci Nanotechnol* **12**, 119-126.
[18] Pellegrino LJ, Pellegrino AS, Cushman AJ (1979) A Stereotaxic Atlas of the Rat Brain Plenum Press, New York.
[19] Arkhipov V, Kapralova M, Pershina E, Gordon R (2014) Delayed treatments with pharmacological modulators of pre- and postsynaptic mGlu receptors rescue the hippocampus from kainate-induced neurodegeneration. *Neurosci Letters* **570**, 5-9.
[20] Andrievsky GV, Bruskov VI, Tykhomyrov AA, Gudkov SV (2009) Peculiarities of the antioxidant and radioprotective effects of hydrated C60 fullerene nanostuctures in vitro and in vivo. *Free Radic Biol Med* **47**, 786-793.
[21] Garai K, Frieden C (2013) Quantitative analysis of the time course of Aβ oligomerization and subsequent growth steps using tetramethylrhodamine-labeled Aβ. *Proc Natl Acad Sci USA* **110**, 3321-3326.
[22] Morris R (1984) Development of a water-maze procedure for studying spatial learning in the rat. *Neurosci Meth* **11**, 47-60.
[23] Vorhees CV, Williams MT (2006) Morris water maze: procedures for assessing spatial and related forms of learning and memory. *Nat Protoc* **1**, 848-858.
[24] Morris RG, Frey U (1997) Hippocampal synaptic plasticity: role in spatial learning or the automatic recording of attended experience? *Philos Trans R Soc Lond B Biol Sci* **352**, 1489-1503.
[25] Iversen LL, Mortishire-Smith RJ, Pollack SJ, Shearman MS (2003) The toxicity in vitro of beta-amyloid protein. *Biochem J* **311**, 1-16.
[26] Frozza RL, Horn AP, Hoppe JB, Simao F, Gerhardt D, Comiran RA, Salbego CG (2009) A comparative study of beta-amyloid peptides Abeta1-42 and Abeta25-35 toxicity in organotypic hippocampal slice cultures. *Neurochem Res* **34**, 295-303.

[27] Plant LD, Boyle JP, Smith IF, Peers C, Pearson HA (2003) The production of amyloid beta peptide is a critical requirement for the viability of central neurons. *J Neurosci* **23**, 5531-5535.
[28] Kühnel W (2003) Color Atlas of Cytology, Histology, and Microscopic Anatomy, 4th edition. Stuttgart: Georg Thieme Verlag; pp. 534.
[29] Vorobyov V, Kaptsov V, Gordon R, Makarova E, Podolski I, Sengpiel F (2015) Neuroprotective Effects of Hydrated Fullerene C60: Cortical and Hippocampal EEG Interplay in an Amyloid-Infused Rat Model of Alzheimer's Disease. *J Alzheimer's Dis* **45**, 217-233.
[30] Klementiev B, Novikova T, Novitskaya V, Walmod PS, Dmytriyeva O, Pakkenberg B, Berezin V, Bock E (2007) A neural cell adhesion molecule-derived peptide reduces neuropathological signs and cognitive impairment induced by $A\beta_{25-35}$. *Neuroscience* **145**, 209-224.
[31] Schmued LC, Hopkins KJ (2000) *Fluoro-Jade B*: a high fluorescent marker for the localization of neuronal degeneration. *Brain Res* **874**, 123-130.
[32] Snyder JS, Radik R, Wojtowicz J, Cameron M, Heather A (2009) Anatomical Gradients of Adult Neurogenesis and Activity: Young Neurons in the Ventral Dentate Gyrus Are Activated by Water Maze Training. *Hippocampus* **19**, 360-370.
[33] Jinno S (2011) Topographic Differences in Adult Neurogenesis in the Mouse Hippocampus: A Stereology-Based Study Using Endogenous Markers. *Hippocampus* **21**, 467–480.
[34] Kroemer G, Galluzzi L, Vandenabeele P et al (2009) Classification of cell death: recommendations of the Nomenclature Committee on Cell Death. *Cell Death Differ* **16**, 3-11.
[35] Cohen NJ, Squire LR (1980) Preserved learning and retention of pattern- analyzing skillin amnesia: dissociation of knowing how and knowing that. *Science* **210**, 207–210.
[36] Stepanichev MY, Zdobnova IM, Zarubenko II, Moiseeva YV, Lazareva NA, Onufriev MV, Gulyaeva NV (2004) Amyloid-beta25-35 -induced memory impairments correlate with cell loss in rat hippocampus. *Physiol Behav* **80**, 647-655.
[37] Selkoe DJ (2008) Soluble oligomers of the amyloid beta-protein impair synaptic plasticity and behavior. *Behav Brain Res* **192**, 106-113.
[38] Zhang SJ, Ye J, Miao C, Tsao A, Cerniauskas I, Ledergerber D, Moser MB, Moser EI (2013) Optogenetic dissection of entorhinal-hippocampal functional connectivity. *Science* **340**, 1232627 (Enhanced Online Article).
[39] Witter M (2010) Connectivity of the hippocampus. In: Cutsuridis V, Graham B, Cobb S, Vida I (eds) Hippocampal microcircuits: a computational modeler's resource book. Springer, New York, pp. 5-26.
[40] Schmidt B, Marrone DF, Markus EJ (2012) Disambiguating the similar: The dentate gyrus and pattern separation. *Behav Brain Res* **226**, 56-65.

[41] Groen Th, Miettinen P, Kadish I (2003) The entorhinal cortex of the mouse: Organization of the projection to the hippocampal formation. *Hippocampus* **13**, 133-149.
[42] Kundrotiene J, Wagner A, Liljequist S (2004) Fluoro-Jade and TUNEL staining as useful tools to identify ischemic brain damage following moderate extradural compression of sensorimotor cortex. *Acta Neurobiol Exp* **64**, 153-162.
[43] Gordon RYa, Shubina LV, Kapralova MV, Pershina EV, Khutsyan SS, Arkhipov VI (2015) Peculiarities of Neurodegeneration of Hippocampus Fields after the Action of Kainic Acid in Rats. *Cell & Tissue Biology* **9**, 141-148.
[44] Damjanac M, Rioux Bilan A, Barrier L, Pontcharraud R, Anne C, Hugon J, Page G (2007) *Fluoro-Jade B* staining as useful tool to identify activated microglia and astrocytes in a mouse transgenic model of Alzheimer's disease. *Brain Res* **1128**, 40-49.
[45] Tuppo EE, Arias HR (2005) The role of inflammation in Alzheimer's disease. *Int J Biochem Cell Biol* **37**, 289-305.
[46] Bagheri M, Rezakhani A, Nystrom S, Turkina M, Roghani M, Hammarstrom P, Mohseni S (2013) Amyloid Beta1-40-Induced Astrogliosis and the Effect of Genistein Treatment in Rat: A Three-Dimensional. *Confocal Morphometric and Proteomic Study. PLoS One* **8**, 1-14 e76526.
[47] Chapuis J, Cohen Y, He X, Zhang Z, Jin S, Xu F, Wilson DA (2013) Lateral Entorhinal Modulation of Piriform Cortical Activity and Fine Odor Discrimination. *J Neurosci* **33**, 13449-13459.
[48] Xu W, Shane FA, Nixon R, Levy E, Wilson DA (2015) Early hyperactivity in lateral entorhinal cortex is associated with elevated levels of AβPP metabolites in the Tg2576 mouse model of Alzheimer's disease. *Exp Neurol* **264**, 82-91.
[49] Hales JB, Schlesiger MI, Leutgeb JK, Squire LR, Leutgeb S, Clark RE (2014) Medial Entorhinal Cortex Lesions Only Partially Disrupt Hippocampal Place Cells and Hippocampus-Dependent Place Memory. *Cell Reports* **9**, 893-901.
[50] Kim S, Sapiurka M, Clark RE, Squire LR (2013) Contrasting effects on path integration after hippocampal damage in humans and rats. *Proc Natl Acad Sci USA* **110**, 4732-4737.
[51] Squire LR (2009) Memory and Brain Systems: 1969–2009. *J Neurosci* **29**, 2711-12716.
[52] Cowan N (2008) What are the differences between long-term, short-term, and working memory? *Progress in Brain Res* **169**, 323-338.
[53] Gorman AM (2008) Neuronal cell death in neurodegenerative diseases: recurring themes around protein handling. *J Cell Mol Med* **12**, 2263-2280.
[54] Kee N, Teixeira CM, Wang AH, Frankland PW (2007) Preferential incorporation of adult generated granule cells into spatial memory networks in the dentate gyrus. *Nat Neurosci* **10**, 355-362.

[55] Bekiari C, Giannakopoulou A, Siskos N, Grivas I, Tsingotjidou A, Michaloudi H, Papadopoulos GC (2015) Neurogenesis in the septal and temporal part of the adult rat dentate gyrus. *Hippocampus* **25**, 511-523.
[56] Palop JJ, Mucke L (2010) Amyloid-β Induced Neuronal Dysfunction in Alzheimer's Disease: From Synapses toward Neural Networks. *Nat Neurosci* **13**, 812–818.
[57] Jessberger S, Clark RE, Broadbent NJ et al (2009) Dentate gyrus-specific knockdown of adult neurogenesis impairs spatial and object recognition memory in adult rats. *Cold Spring Harbor Laboratory Press, Learning & Memory* **16**, 147-154.
[58] Dugan LL, Turetsky DM, Du C et al (1997) Carboxyfullerenes as neuroprotective agents. *Proc Natl Acad Sci USA* **94**, 9434-9439.
[59] Podolski IYa, Podlubnaya ZA , Godukhin, OV. 2010. Fullerenes C60, antiamyloid action, the brain, and cognitive processes. *Biophysics* **55**, 1-76.
[60] Bobylev AG, Kornev AB, Bobyleva LG et al (2011) Fullerenolates: metallated polyhydroxylated fullerenes with potent anti-amyloid activity. *Org Biomol Chem* **9**, 5714-5719.
[61] Wen Y-Y, Wen L-P, Wang M (2014) The role of low levels of fullerene C60 nanocrystals on enhanced learning and memory of rats through persistent CaMKII activation. *Biomaterials* **35**, 9269-9279.
[62] Hoey SE, Buonocore F, Cox CJ, Hammond VJ, Perkinton MS, Williams RJ (2013) AMPA Receptor Activation Promotes Non-Amyloidogenic Amyloid Precursor Protein. *Processing and Suppresses Neuronal Amyloid-b Production. PLoS One* **8**, e78155.
[63] Jin H, Chen WQ, Tang XW, Chiang LY, Yang CY, Schloss JV, Wu JY (2000) Polyhydroxylated C(60), fullerenols, as glutamate receptor antagonists and neuroprotective agents. *J Neurosci Res* **62**, 600-607.
[64] Oseki T, Monteforte PT, Pereira GJS, Hirata H, Ureshino RP, Bincoletto C, Hsu Y-T, Smaili SS (2014) Apoptosis induced by Aβ25–35 peptide is Ca2+-IP3 signaling-dependent in murine astrocytes. *Eur J Neuroscience* **40**, 3, 2471–2478.
[65] Sayes CM, Gobin AM, Ausman KD, Mendez J, West JL, Colvin VL (2005) Nano-C60 cytotoxicity is due to lipid peroxidation. *Biomaterials* **26**, 7587-7595.
[66] Matthews PM, Filippini N, Douaud G (2013) Brain structural and functional connectivity and the progression of neuropathology in Alzheimer's disease. *J Alzheimer's Dis* **33** Suppl 1, S163-S172.
[67] Wisse LE, Reijmer YD, ter Telgte A, Kuijf HJ, Leemans A, Luijten PR, Koek HL, Geerlings MI, Biessels GJ; Utrecht Vascular Cognitive Impairment (VCI) Study Group (2015) Hippocampal disconnection in early Alzheimer's disease: a 7 tesla MRI study. *J Alzheimer's Dis* **45**, 1247-1256.

**Figure legends**

**Figure 1.** Trial-by-trial learning progression (A, B) and memory evaluation (C - F) in rats on different days after intrahippocampal injections of saline, $A\beta_{35-25}$, $A\beta_{25-35}$, and $C_{60}$HyFn in combinations of Saline + Saline *vs.* Saline + $A\beta_{35-25}$ and $C_{60}$HyFn + $A\beta_{25-35}$ *vs.* Saline + $A\beta_{25-35}$. Session I is a composite of the experiments performed on Days 14 and 21 (1 - 4 and 5 - 8 trials, respectively) with the hidden platform invariably located in one of the pool's quadrants. In sessions of II, III, and IV (on Days 28, 35, and 42, respectively) the rats experienced a *reversal learning* of 4 trials with the hidden platform in another quadrant, individually for each rat across the days. Abscissa enumerates the training trials (A, B), the learning sessions (C, D), and testing intervals (in hours) after the session (E, F); ordinate is time needed to reach the platform (A - D) and time spending in target quadrant (E, F), both in seconds. Horizontal dashed lines on E and F denote time values randomly distributed between all (four) pool's quadrants. Diamond denotes significant difference between groups of rats in corresponding session ($p < 0.05$, Wilcoxon test). Error bars show 1 SEM.

**Figure 2.** Microphotograph of a coronal brain section of a naïve rat at the level of dorsal hippocampus stained with cresyl violet. "Supra" and "infra" denote supra- and infra-pyramidal blades of the dentate gyrus (DG); CA1, CA3, and CA4 denote areas of the hippocampus. Scale bar is 500 μm.

**Figure 3.** Microphotographs of dorsal hippocampus (area CA1) sections stained with cresyl violet in two rats from different groups on Day 14 after intrahippocampal infusion of Saline + $A\beta_{25-35}$ (A) and $C_{60}$HyFn + $A\beta_{25-35}$ (B). Arrowheads on A indicate representative swelled and vacuolated cells with indistinct and ruptured cellular and nuclear membranes. Pretreatment with fullerene $C_{60}$HyFn, 2 h prior to $A\beta_{25-35}$, partially prevented these pathological effects of $A\beta_{25-35}$ on CA1 cells. Arrowheads on B indicate three representative cells within other morphologically intact neurons characterized by uniformly colored cytoplasm and distinct nucleolus and membranes. Scale bars are 40 μm.

**Figure 4.** Microphotographs of dorsal hippocampus (area CA3) sections stained with cresyl violet in the rat after intrahippocampal infusion of Saline + $A\beta_{25-35}$ on Day 14. On B, the boxed area from A is shown at higher magnification. Note the pathological changes in neurons similar to those observed in CA1 (see Fig. 4A) and typical lyzing effect on cells (arrowheads on B). Scale bars are 50 μm on A and 20 μm on B.

**Figure 5.** Populations of morphologically intact neurons in CA1 and CA3 areas of the hippocampus of rats on Day 14 after intrahippocampal injections with Saline + Saline, Saline

+ $A\beta_{25-35}$, $C_{60}$HyFn + $A\beta_{25-35}$ or $C_{60}$HyFn + Saline (white, black, gray or shaded bars, respectively). Stars denote significant differences between Saline + $A\beta_{25-35}$ and other groups (with exception of CA 3 in rats from in $C_{60}$HyFn + $A\beta_{25-35}$ group), ** - $p < 0.01$, *** - $p < 0.001$, Wilcoxon test. + denotes significant ($p < 0.05$) difference between CA3 of rats from Saline + Saline and $C_{60}$HyFn + $A\beta_{25-35}$ groups

**Figure 6.** Microphotographs of dentate gyrus sections stained with cresyl violet in four rats from different groups on Day 14 (A, C) and Day 45 (B, D) after intrahippocampal infusion of Saline + $A\beta_{25-35}$ (A, B) and $C_{60}$HyFn + $A\beta_{25-35}$ (C, D). "Supra" and "infra" denote supra- and infra-pyramidal blades of the dentate gyrus (DG); CA1 and CA4 denote areas of the hippocampus. On Day 14, note significant damage of DG supramedial bundle induced by $A\beta_{25-35}$ (A) and partial preservation of the bundle by the fullerene (C). On Day 45, the DG suprapyramidal bundle was completely restored after $A\beta_{25-35}$ injection (B), while after $C_{60}$HyFn pretreatment, the bundle was partially restored (D). Scale bars are 500 μm.

**Figure 7.** Microphotographs of brain sections from the rat intrahippocampally infused with Saline + $A\beta_{25-35}$ (Day 14) and stained by either antibodies against $A\beta_{1-42}$ (A) or *Fluoro-Jade B* (B). Note $A\beta_{1-42}$ accumulation in cytoplasm of CA1 neurons (arrowheads on A) and *Fluoro-Jade B* fluorescence around the "black holes" shown by arrowheads on B, supposedly, in glia (triangles). Scale bars are 50 μm.

**Figure 8.** Microphotographs of dentate gyrus (A) and hippocampal CA3 (B) sections stained with *Fluoro-Jade B* in the rat from Saline + $A\beta_{25-35}$ group on Day 14. Supra" and "infra" denote supra- and infrapyramidal blades of the dentate gyrus (DG); CA3 denote areas of the hippocampus. In DG, *Fluoro-Jade B* was captured by both glia and degenerated neurons, especially, in the supra- vs. infrapyramidal bundles (arrowheads on A) Note that in CA3, the fluorescence was observed around, rather than inside, the bodies of pyramidal neurons ("black holes" shown by arrowheads on B), supposedly, in glia (white triangles). Scale bars are 400 μm.

**Figure 9.** Populations of morphologically intact neurons in CA1 and CA3 areas of the hippocampus of rats on Day 45 after intrahippocampal injections with Saline + Saline, Saline + $A\beta_{25-35}$, $C_{60}$HyFn + $A\beta_{25-35}$ or $C_{60}$HyFn + Saline (white, black, gray or shaded bars, respectively). Stars denote significant differences between Saline + $A\beta_{25-35}$ and other groups, ** - $p < 0.01$, *** - $p < 0.001$, Wilcoxon test. + denotes significant ($p < 0.05$) difference between CA3 of rats from Saline + Saline and $C_{60}$HyFn + $A\beta_{25-35}$ groups.

**Figure 10.** Microphotographs of hippocampal CA3 (A, B) sections stained with cresyl violet in two rats from different groups on Day 45 after intrahippocampal infusion of Saline + $A\beta_{25-35}$ (A) and $C_{60}$HyFn + $A\beta_{25-35}$ (B). Arrowheads on A indicate representative swelled and vacuolated cells with indistinct and ruptured cellular and nuclear membranes. Pretreatment with fullerene $C_{60}$HyFn, 2 h prior to $A\beta_{25-35}$, partially prevented these pathological effects of $A\beta_{25-35}$ on CA3 cells. Arrowheads on B indicate the cells within a large amount of morphologically intact neurons with uniformly colored cytoplasm and distinct nucleolus and membranes. Scale bars are 20 μm.

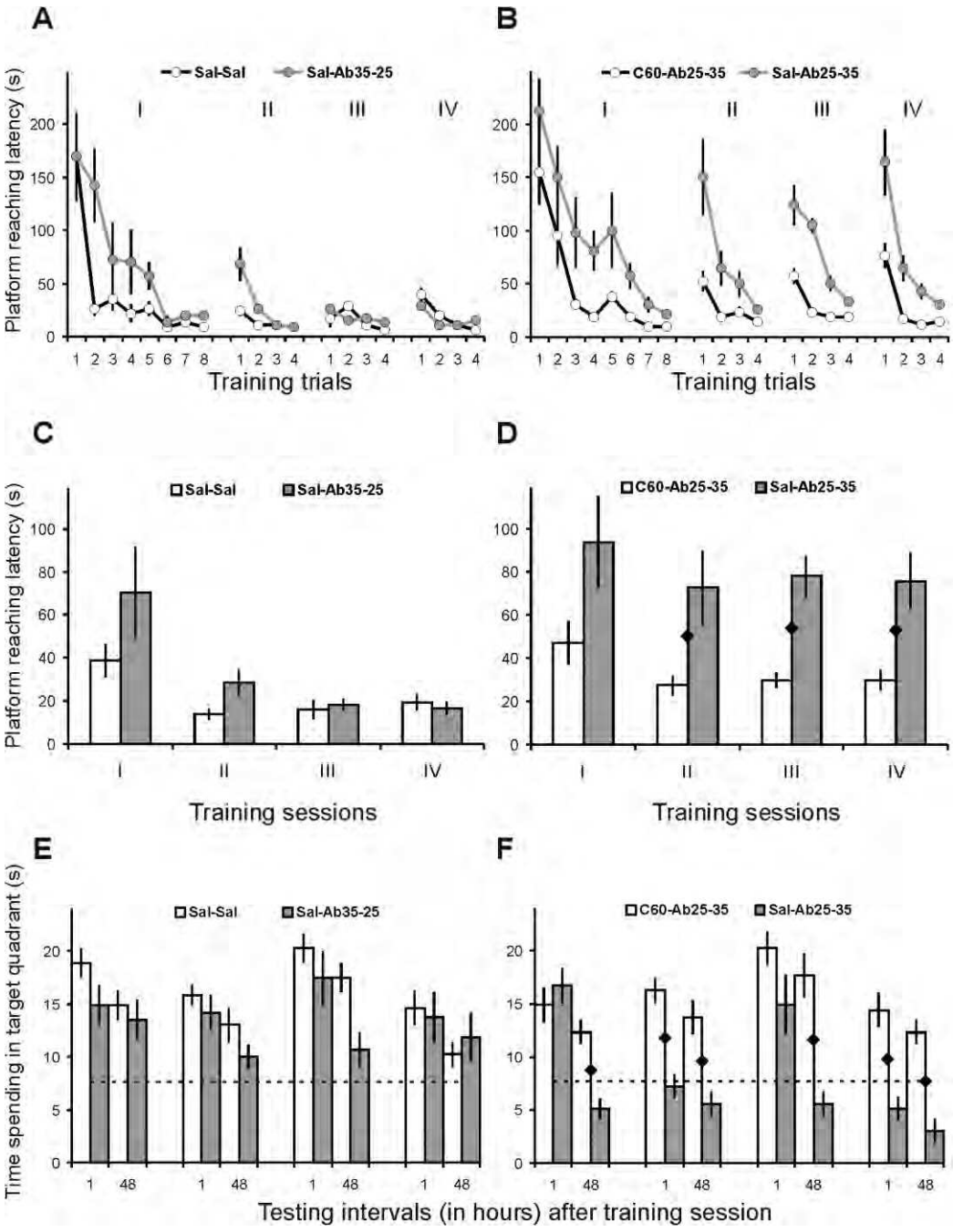
A
Sal-Sal
Sal-Ab35-25
Platform reaching latency (s)
Training trials
B
C60-Ab25-35
Sal-Ab25-35
Training trials
C
Sal-Sal
Sal-Ab35-25
Platform reaching latency (s)
Training sessions
D
C60-Ab25-35
Sal-Ab25-35
Training sessions
E
Sal-Sal
Sal-Ab35-25
Time spending in target quadrant (s)
Testing intervals (in hours) after training session
F
C60-Ab25-35
Sal-Ab25-35

Figure 1

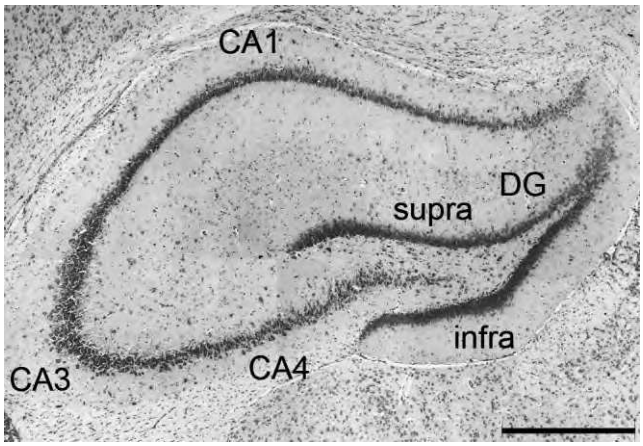


Figure 2

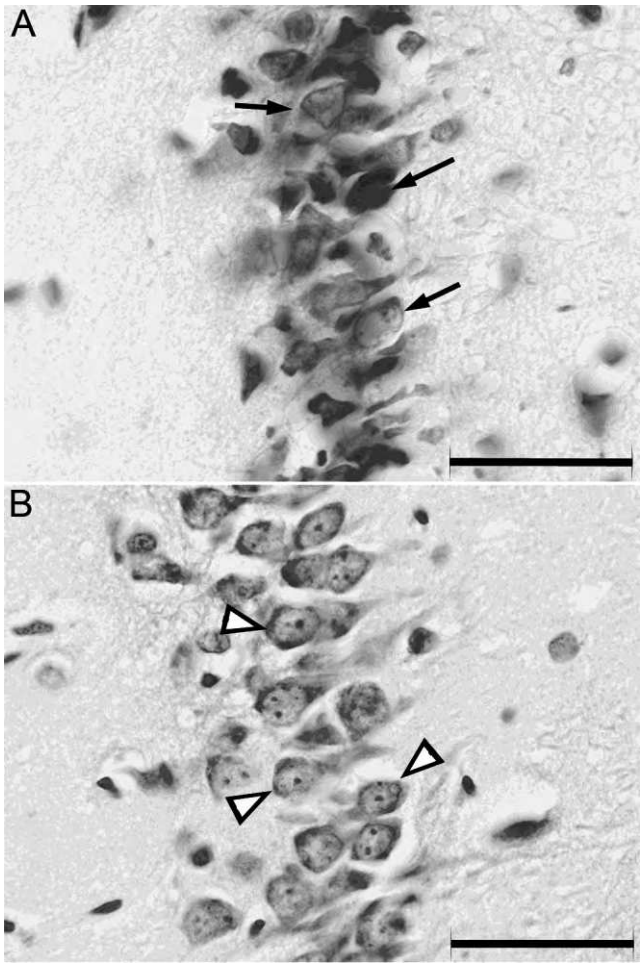


Figure 3

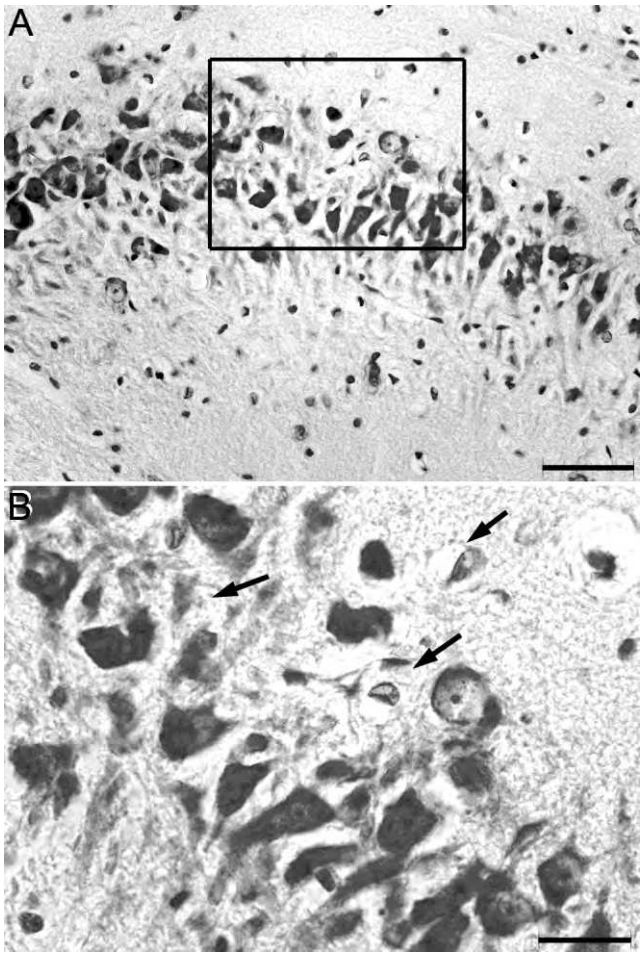


Figure 4

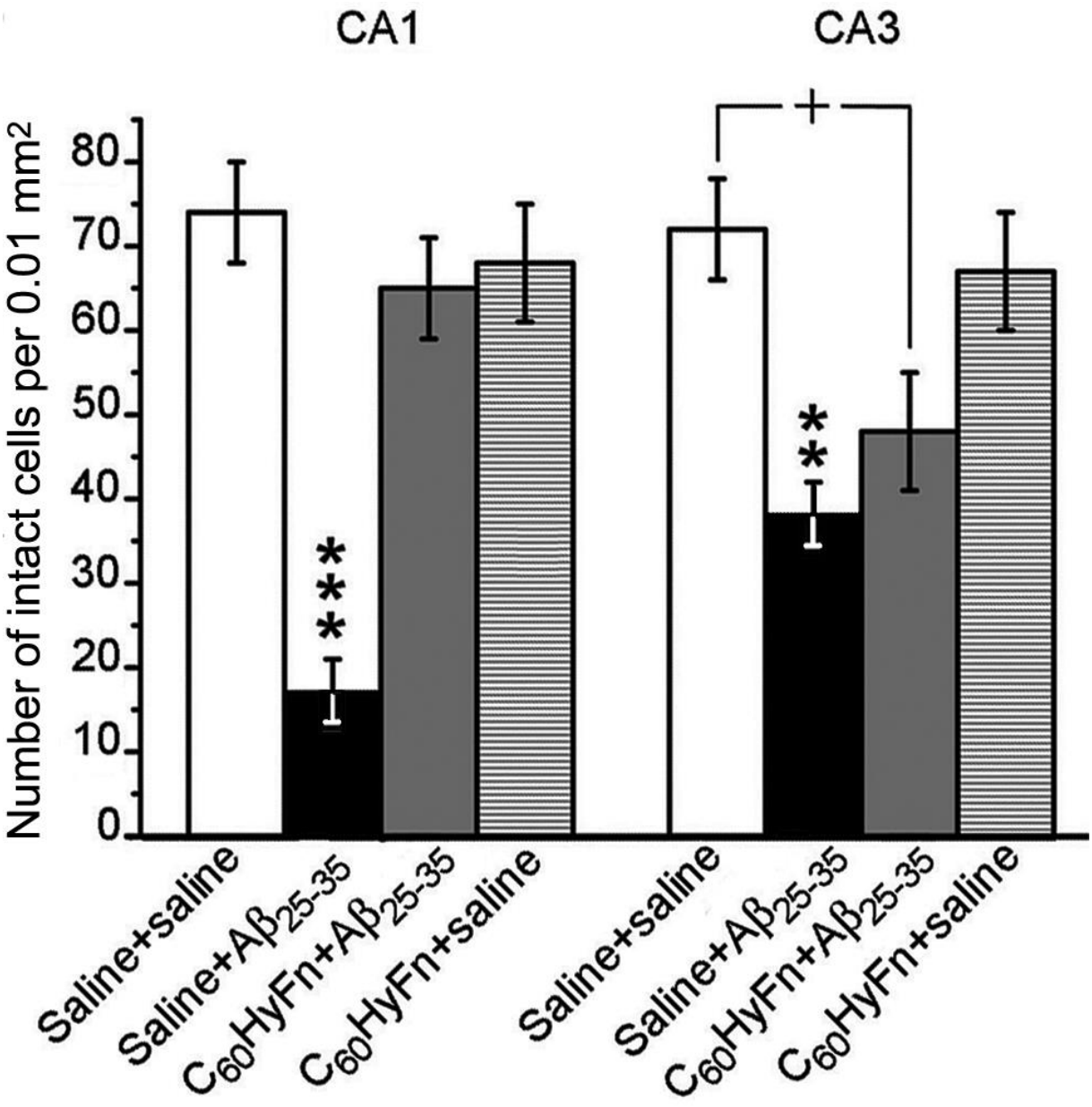
CA1
CA3
Number of intact cells per 0.01 mm²
80
70
60
50
40
30
20
10
0
***
**
+
Saline+saline
Saline+Aβ25-35
C60HyFn+Aβ25-35
C60HyFn+saline
Saline+saline
Saline+Aβ25-35
C60HyFn+Aβ25-35
C60HyFn+saline

Figure 5

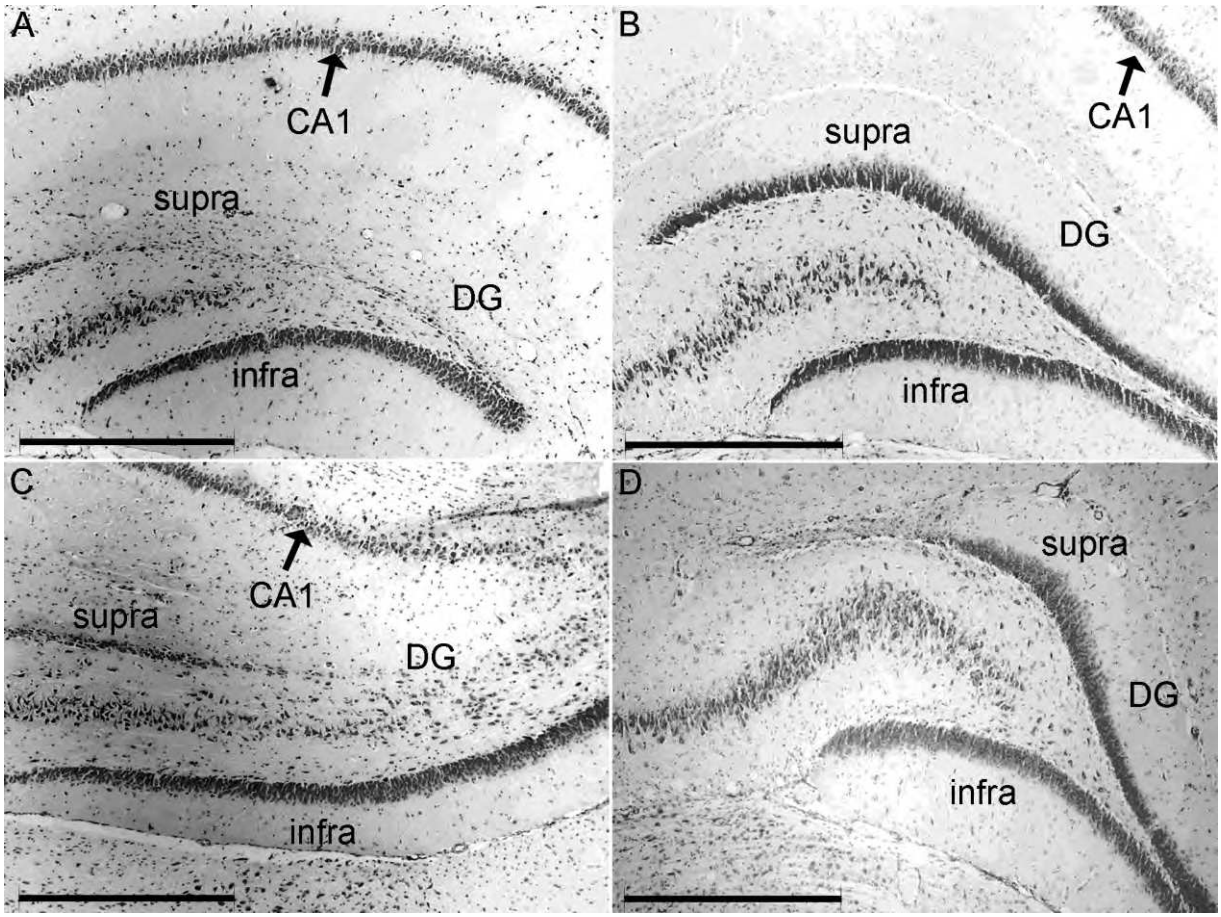
A
CA1
supra
DG
infra
B
CA1
supra
DG
infra
C
CA1
supra
DG
infra
D
supra
DG
infra

Figure 6

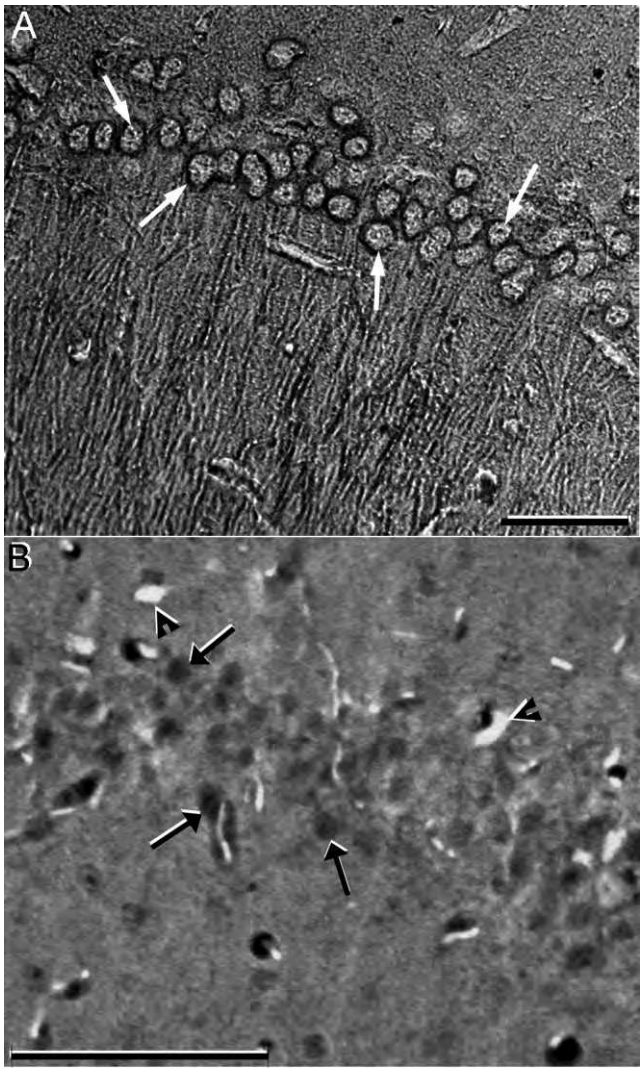


Figure 7

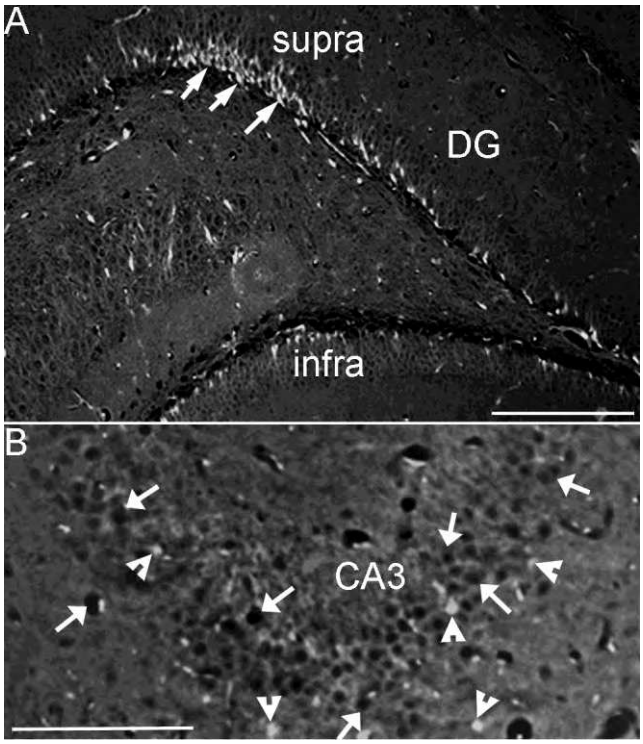


Figure 8

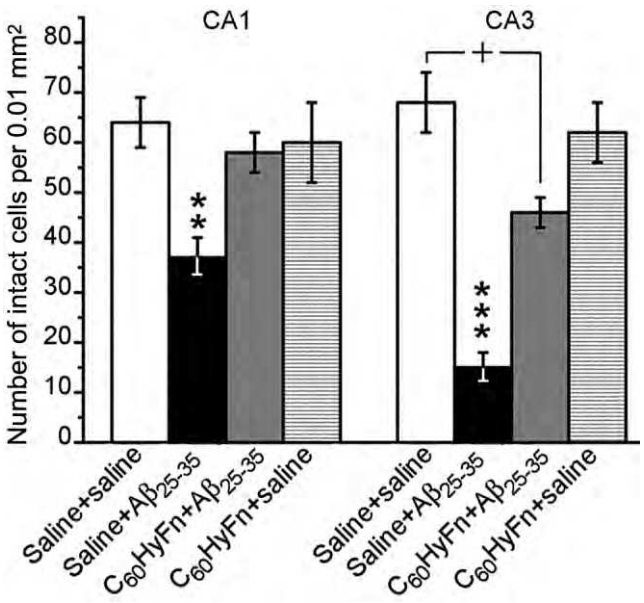
CA1
CA3
Number of intact cells per 0.01 mm²
80
70
60
50
40
30
20
10
0
**
***
+
Saline+saline
Saline+Aβ25-35
C60HyFn+Aβ25-35
C60HyFn+saline
Saline+saline
Saline+Aβ25-35
C60HyFn+Aβ25-35
C60HyFn+saline

Figure 9

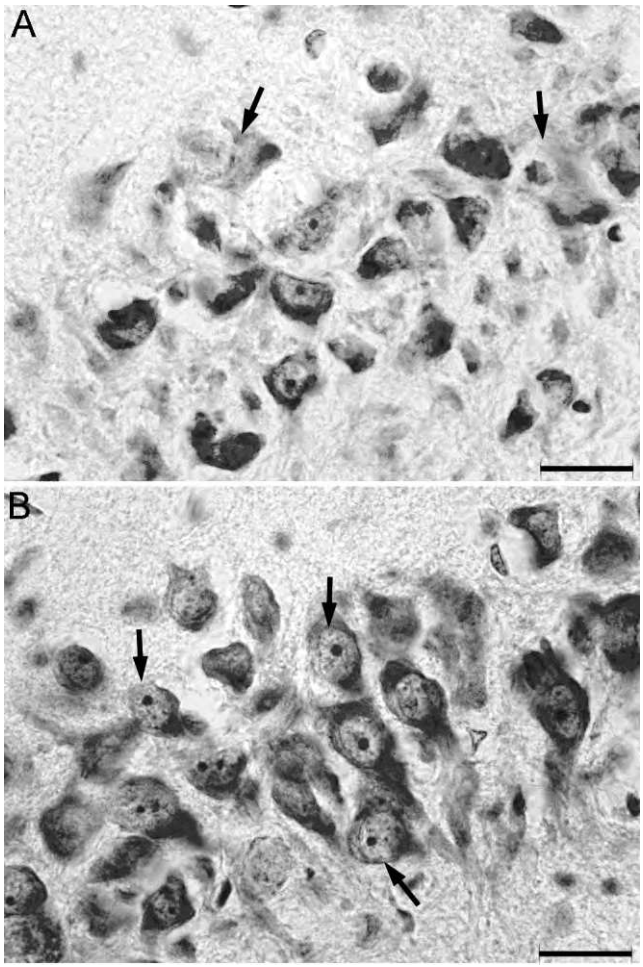


Figure 10